Application of: Gabor Forgacs et al. Art Unit: 1653
Serial No.: 10/590,446
Filed: October 10, 2007
Confirmation No.: 8467
For: SELF-ASSEMBLING CELL AGGREGATES AND METHODS OF MAKING ENGINEERED TISSUE USING THE SAME
Examiner: Srivastava, Kailash C.

DECLARATION OF PRIOR INVENTION UNDER 37 C.F.R. § 1.131

We, Gabor Forgacs, Karoly Jakab, Adrian Neagu, and Vladimir Mironov, declare as follows:

1. We are the co-inventors of the subject matter claimed in the above-referenced patent application, U.S. Patent Application Serial No. 10/590,466 (the '466 application).

2. We conceived of and reduced to practice the subject matter of the invention as claimed in pending independent claim 52 prior to October 4, 2003. Exhibits A and B attached hereto are submitted as evidence of our conception and reduction to practice prior to October 4, 2003.

3. Exhibit A is a true and correct copy of an article by Jakab et al., which was published in the journal *Proceedings of the National Academy of Sciences (PNAS)* on March 2, 2004. The face of the article indicates that a manuscript for the article was received for review by the journal on July 20, 2003. We are all co-authors of this article, and conceived of and reduced to practice the subject matter described therein.

4. Exhibit B is a true and correct copy of the manuscript for the Jakab et al. article originally submitted to the journal *PNAS*. It will be appreciated that the manuscript as originally submitted to the journal *PNAS* is substantially similar to the published Jakab et al. article, and that both documents describe the subject matter of

independent claim 52 of the '466 application.[1] In particular, the manuscript describes: a three-dimensional layered structure comprising at least one layer of a matrix; and a plurality of cell aggregates, each cell aggregate comprising a plurality of living cells; wherein the cell aggregates are embedded in the at least one layer of matrix in a non-random predetermined pattern, the cell aggregates having predetermined positions in the pattern (see, e.g., p. 2, lines 16–17 & 21–23; p. 4, line 21–p. 6, line 18; p. 14, lines 7–13, p. 25, lines 1–11; and Figure 3).

5. Based on the foregoing, we believe that we conceived of and reduced to practice the claimed invention prior to October 4, 2003.

6. All work referred to herein was carried out in the United States.

7. We further declare that all statements made herein of our own knowledge are true and that all statements made on information and belief are believed to be true; and further, that these statements were made with the knowledge that willful false statements and the like so made are punishable by fine or imprisonment, or both, under 18 U.S.C. § 1001, and that such willful false statements may jeopardize the validity of the application or any patent issuing thereon.

12/30/11
Date

Gabor Forgacs

[1] Figure 1 of the manuscript as originally filed could not be located, but was substantially similar to Figure 1 of the Jakab et al. article as published, the primary difference being that Figure 1 as published included an additional collagen concentration (1.2 mg/ml). This is clear from a comparison of the figure legends for Figure 1 in the manuscript (page 25) and the published article (page 2866).

12/29/2011
Date

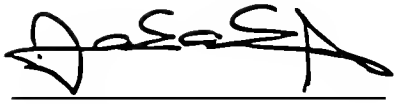
Karoly Jakab

DEC, 30, 2011
Date

Adrian Neagu

12/31/11
Date

Vladimir Mironov

Engineering biological structures of prescribed shape using self-assembling multicellular systems

Karoly Jakab*, Adrian Neagu*†, Vladimir Mironov‡, Roger R. Markwald‡, and Gabor Forgacs*§¶

Departments of *Physics and §Biology, University of Missouri, Columbia, MO 65211; †Department of Biophysics and Medical Informatics, Victor Babes University of Medicine and Pharmacy, 1900 Timisoara, Romania, and ‡Department of Cell Biology and Anatomy, Medical University of South Carolina, Charleston, SC 29425

Communicated by Joel L. Lebowitz, Rutgers, The State University of New Jersey, Piscataway, NJ, January 8, 2004 (received for review July 20, 2003)

Self-assembly is a fundamental process that drives structural organization in both inanimate and living systems. It is in the course of self-assembly of cells and tissues in early development that the organism and its parts eventually acquire their final shape. Even though developmental patterning through self-assembly is under strict genetic control it is clear that ultimately it is physical mechanisms that bring about the complex structures. Here we show, both experimentally and by using computer simulations, how tissue liquidity can be used to build tissue constructs of prescribed geometry *in vitro*. Spherical aggregates containing many thousands of cells, which form because of tissue liquidity, were implanted contiguously into biocompatible hydrogels in circular geometry. Depending on the properties of the gel, upon incubation, the aggregates either fused into a toroidal 3D structure or their constituent cells dispersed into the surrounding matrix. The model simulations, which reproduced the experimentally observed shapes, indicate that the control parameter of structure evolution is the aggregate–gel interfacial tension. The model-based analysis also revealed that the observed toroidal structure represents a metastable state of the cellular system, whose lifetime depends on the magnitude of cell–cell and cell–matrix interactions. Thus, these constructs can be made long-lived. We suggest that spherical aggregates composed of organ-specific cells may be used as "bio-ink" in the evolving technology of organ printing.

Self-assembly is the fundamental process, which generates structural organization across scales (1). Histogenesis and organogenesis are examples of self-assembly processes, in which, through cell–cell and cell–extracellular matrix interactions, the developing organism and its parts gradually acquire their final shape. In the present work we use both experimental and computational approaches to demonstrate how the self-organizing properties of cells and tissues, the basis for morphogenesis, can be exploited to build 3D biological structures of prescribed geometry.

Tissue engineering (2–7) offers the opportunity to study self-assembly processes during histo- and organogenesis *in vitro*, under controlled conditions. Tissue engineering aims not only to create desirable organs, but also to better understand the fundamental mechanisms and principles of biological organization in general and morphogenesis in particular. Classical tissue engineering is based on seeding cells into biodegradable polymer scaffolds or gels, culturing and expanding them in bioreactors for several weeks, and finally implanting the resulting tissue into the recipient organism, where the maturation of the new organ takes place.

It has recently been suggested to use cell aggregates, instead of individual cells, as building blocks in tissue engineering (8, 9). Cell aggregates have traditionally been used as a powerful tool to understand the principles of cell–cell (10) and cell–matrix adhesion (11), as well as cell sorting (12). In addition, rapid prototyping technology has successfully been applied for computer-aided deposition of cells in gels to create 3D tissue constructs (13, 14). We suggest that cell aggregates may be used as drops of "bio-ink," which, upon implantation or "printing" into a scaffold ("bio-paper"), have the ability to fuse into 3D organ structures (15–17).

The ability of cell aggregates to fuse is based on the concept of tissue fluidity (18, 19), according to which embryonic tissues in many respects can be considered as liquids. In particular, in suspension or on nonadhesive surfaces, various multicellular aggregates round up into spherical shape similarly to liquid droplets (12). We hypothesize that closely placed aggregates in appropriately chosen 3D gels can fuse to form tissue constructs of desired geometry.

To demonstrate the feasibility of such a proposition, we used aggregates of genetically transformed cells with controlled adhesive properties, and arranged them to form a ring in gels of different chemical and mechanical properties. Our results demonstrate that contiguous aggregates under appropriate conditions, defined by the composition of the embedding gel, indeed can fuse into structures of specified morphology. We have also constructed and experimentally validated a mathematical model of cell aggregate fusion.

Taken together, these results suggest that cell aggregates can successfully be used as building blocks in tissue engineering technologies. They also provide support for the concept of self-assembling bio-ink, and thus justification for the use of cell aggregates in the evolving organ printing tools.

Materials and Methods

Cell Aggregate Preparation. Chinese Hamster Ovary (CHO) cells, transfected with *N*-cadherin (courtesy of A. Bershadsky, Weizmann Institute, Rehovot, Israel), were infected with histone binding H2B-YFP retrovirus (kindly provided by R. D. Lansford, Beckman Institute at California Institute of Technology). Confluent cell cultures (3–4 $\times$ 10^6 cells per 75-cm^2 TC dish) grown in DMEM (GIBCO/BRL) supplemented with 10% FBS (U.S. Bio-Technologies, Pottstown, PA), 10 μg/ml penicillin, streptomycin, gentamicin, and kanamycin, 400 μg/ml geneticin), were washed twice with Hanks' balanced salt solution (HBSS) containing 2 mM $CaCl_2$, then treated for 10 min with trypsin 0.1% (diluted from 2.5% stock, GIBCO/BRL). Depleted cells were centrifuged at 2,500 rpm for 4 min (Fisher Centrific model 225). The resulting pellet was transferred into capillary micropipettes of 500-μm diameter and incubated at 37°C with 5% CO_2 for 10 min. The firm cylinders of cells removed from the pipettes were cut into fragments (500-μm height), then incubated in 10-ml tissue culture flasks (Bellco Glass, Vineland, NJ) with 3 ml of DMEM on a gyratory shaker at 120 rpm with 5% CO_2 at 37°C for 24–36 h. This procedure reproducibly provides spherical aggregates of similar size ($\approx$500-μm diameter).

Abbreviations: CHO, Chinese hamster ovary; MCS, Monte Carlo step; DAH, differential adhesion hypothesis.

¶To whom correspondence should be addressed. E-mail: forgacsg@missouri.edu.

www.pnas.org/cgi/doi/10.1073/pnas.0400164101

Cell Aggregate–Gel Structures. NeuroGel (a biocompatible porous poly[*N*-(2-hydroxypropyl)methacrylamide] hydrogel) disks of 10-mm diameter and 2-mm thickness, containing Arg-Gly-Asp (RGD) fragments (kindly provided by Stephane Woerly, Organogel Canada, Quebec) were washed three times with DMEM to eliminate the storage medium. This gel has been shown to provide favorable conditions for spinal cord repair (20, 21). A 0.5-mm wide, 0.5-mm deep circular groove was cut into a disk, then filled with 10 aggregates, placed contiguously to form a closed circle. The groove was refilled with the gel to completely embed the aggregates. This structure was incubated at 37°C, 5% CO_2 for 72 h in a tissue culture dish containing 10 ml of DMEM, washed with PBS, and finally embedded in Tissue-Tek OCT Compound (Electron Microscopy Sciences, Fort Washington, PA). The structure was slowly cooled (1°C per min) to −20°C in a Nalgene freezing container (Nalgene Labware, Rochester, NY). To visualize aggregate fusion at the end of the experiment, cryosectioning was performed with a Reichert 2800N Frigocut cryotome (Reichert Jung, Arnsberg, Germany), yielding 10- to 16-μm-thin slices mounted on microscope slides. Slices were examined on an Olympus IX-70 inverted microscope with fluorescent attachment at ×4 magnification.

To tune the strength of cell–gel interaction, further fusion experiments were conducted in rat-tail collagen type I (Sigma). Collagen was dissolved in 1 M acetic acid, then treated with Ham's F12 medium with sodium bicarbonate. At room temperature, this mixture gels in a few minutes depending on concentration. The gel–aggregate structure was achieved by creating a ring of 10 aggregates on the top of a previously (almost) solidified collagen layer, then covering with liquid collagen that embedded the aggregates after gelation. These samples were incubated under the same conditions as described above. Working with 1.0, 1.2, and 1.7 mg/ml collagen, the samples were transparent; thus, it was possible to follow pattern evolution in time by phase contrast and fluorescent microscopy.

Cell survivability was checked with Trypan Blue (GIBCO/BRL) at the end of each fusion experiment. A minimal number of uniformly distributed dead cells were found.

Modeling Structure Formation by Means of Cell Aggregate Fusion. To investigate shape changes of the evolving pattern, we constructed a simple 3D model, in which the sites of a cubic lattice are occupied either by point-like cells or gel volume elements. The total interaction energy, E of the system is written as

$$E = \sum_{\langle r,r' \rangle} J(\sigma_r, \sigma_{r'}), \qquad [1]$$

where r and r' label lattice sites, and $\langle r, r' \rangle$ signifies summation over neighboring sites, each pair counted once. First, second, and third nearest neighbors are included, and we assume that a cell interacts with the same strength with all of the 26 cells it comes into contact with. To specify occupancy, we assign a spin value, σ, to each lattice site with values 0 for a "gel particle" and 1 for a cell. The interaction energy of two neighbors, $J(\sigma_r, \sigma_{r'})$, may take either of the values $J(0, 0) = -\varepsilon_{gg}$, $J(1, 1) = -\varepsilon_{cc}$, or $J(0, 1) = J(1, 0) = -\varepsilon_{cg}$. Here the positive parameters ε_{gg}, ε_{cc}, and ε_{cg} account for contact interaction strengths for cell–cell, gel–gel, and cell–gel pairs, respectively. More specifically, these are mechanical works needed to disrupt the corresponding bonds. (Note that ε_{cc} and ε_{gg} are works of cohesion, whereas ε_{cg} is work of adhesion per bond; ref. 22.) The strength of cell–cell interaction may be determined experimentally either directly (23) or by measuring the tissue surface tension (12, 24). The cell–gel interaction is tunable via the concentration of RGD groups in the gel (6, 25) or by the concentration of collagen. The gel–gel "bond energy" is an effective measure of gel filament density, interaction, and stiffness. It is determined by the specific chemistry of the gel.

The energy in Eq. 1 may be rewritten by separating interfacial and bulk terms in the sum. As a result we obtain

$$E = \gamma_{cg} B_{cg} + \text{const.} \qquad [2]$$

Here, B_{cg} is the total number of cell–gel bonds, and $\gamma_{cg} = (\varepsilon_{cc} + \varepsilon_{gg})/2 - \varepsilon_{cg}$ is proportional to the cell–gel interfacial tension (22, 26, 27). The remaining terms in E do not change as the cellular pattern evolves. Our model is inspired by earlier efforts aiming at computer simulations of cell sorting (26–28), the morphogenetic phenomenon in which one of two, initially randomly intermixed cell populations sorts out and becomes surrounded by the other.

The evolution of the system is followed by using Monte Carlo simulations (29), relying on a random number generator of L'Ecuyer with Baym–Durham shuffle (30). The program identifies the cells on the aggregate–gel interface, picks one of them randomly, and exchanges it with an adjacent gel particle chosen by chance. The corresponding change in adhesive energy, ΔE, is calculated, and the new configuration is accepted with a probability $P = 1$ if $\Delta E \leq 0$ or $P = \exp(-\beta \Delta E)$ if $\Delta E > 0$. $\beta = 1/E_T$ is the inverse of the average biological fluctuation energy E_T, analogous to the thermal fluctuation energy (31), $k_B T$ (where k_B is Boltzmann's constant and T is the absolute temperature). In statistical mechanics, this energy characterizes thermal agitation in a system of atoms or molecules. In the case of cells, it is a measure of the spontaneous, cytoskeleton-driven motion of cells, able to break adhesive bonds between neighbors via membrane ruffling (32), or more generally, via membrane protrusive activity (e.g., filopodial extensions). By definition, a Monte Carlo step (MCS) or "unit of time," is completed when each cell in contact with the gel has been given the chance to move once. During each MCS, the interfacial sites are selected in random order. The gel boundary is treated as a fixed physical limit of the system, and cells are constrained to move within the gel.

Results

Structure Formation: Simulations. The result stated in Eq. 2 indicates that the evolution of the cellular pattern is governed by a single parameter, γ_{cg}/E_T, which, for cells with specific adhesion apparatus, is controlled by the chemistry of the gel. The theoretical analysis shows that, once gel properties are appropriately tuned, efficient fusion of adjacent aggregates takes place. This is illustrated in the simulation shown in Fig. 1. For small γ_{cg}/E_T (= 0.25 in Fig. 1 *K* and *L*), cells can spread in the bulk of the gel (i.e., permissive gel) and the pattern evolves toward its lowest energy state, being a sphere. (Because the interfacial energy is small in comparison to the fluctuation energy, the spheroidal structure in Fig. 1*L* is rather disperse.) Under optimal cell–gel interface properties, expressed in our model by a certain range in γ_{cg}/E_T, fusion of aggregates results in a 3D toroidal structure. An example of this kind is depicted in Fig. 1 *A* and *B* ($\gamma_{cg}/E_T = 0.9$, nonpermissive gel).

Energetics During Structure Formation. Some shapes correspond to local minima of the interaction energy. These represent metastable configurations. They are identified from plateaus in the plot of the total interaction energy vs. MCS, and are important for tissue engineering, for they can be made long-lived. This is illustrated in more detail in the simulation shown in Fig. 2, where the initial state progresses toward a metastable toroidal configuration, whose energy is essentially unchanged in the entire interval between 10^4 and 6×10^4 MCS (Fig. 2*A*). Eventually the toroid becomes unstable, and at $\approx 10^5$ MCS it ruptures (Fig. 2*B*). Subsequent massive rearrangements lead to a pronounced en-

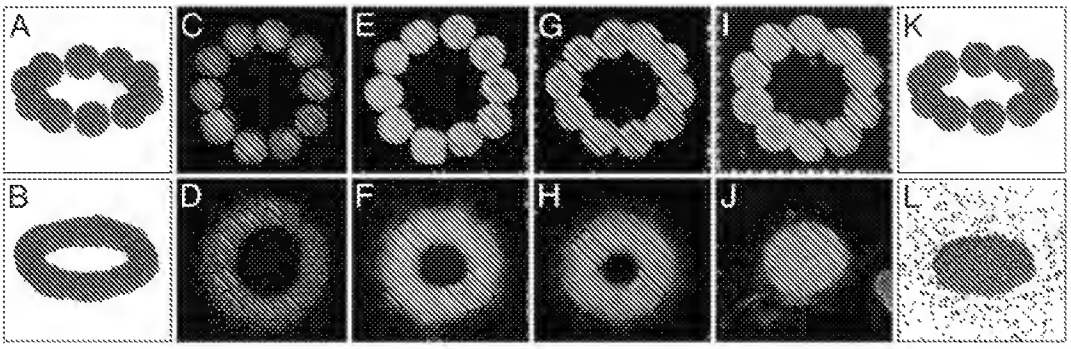

Fig. 1. Initial (*Upper*) and final (*Lower*) cell aggregate configurations in the simulations and in experiments using various biocompatible gels. Panels *A* and *B* correspond to simulations with $\gamma_{cg}/E_T = 0.9$, and *K* and *L* correspond to simulations with $\gamma_{cg}/E_T = 0.25$. The 10 aggregates, each containing 925 cells, are one cell diameter from each other in the starting configurations. The final configurations are reached after 25,000 and 50,000 MCS, respectively. *C–J* correspond to CHO cell aggregates embedded in a neurogel with RGD fragments (*C* and *D*) and collagen gels of concentration 1.0 (*E* and *F*), 1.2 (*G* and *H*), and 1.7 (*I* and *J*) mg/ml. The nuclei of the cells are fluorescently labeled (see *Materials and Methods*), and the images of the cellular patterns were acquired with a ×4 objective. The average diameter of the aggregates is 500 μm.

ergy decrease while the system evolves into three rounded aggregates. These remain stable for a long time because large spatial separations hinder their fusion into a single spheroid. Similar simulations showed that metastability depends on both system size and interaction strengths. Because the evolution of the cellular pattern is driven exclusively by energy minimization, and "time" is measured in MCS, in its present form, the model cannot provide information on the true dynamical behavior of the system.

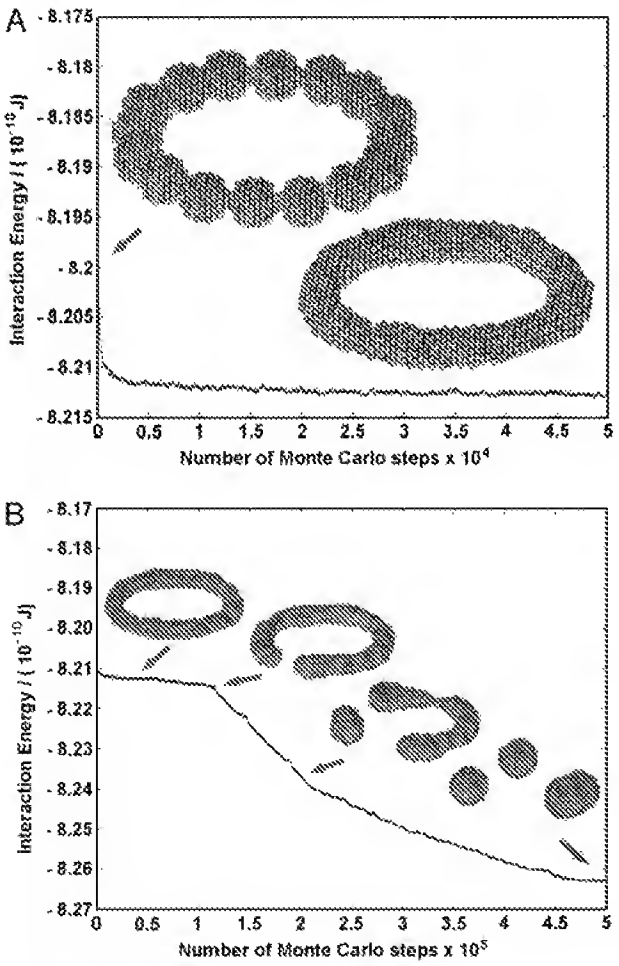

Fig. 2. (*A*) Metastable configuration at $\gamma_{cg}/E_T = 1.1$. Fusion of 16 contiguous aggregates (123 cells each) takes place within the first 5,000 MCS. The plateau of the energy vs. MCS corresponds to a torus. (*B*) The evolution of the energy during 5×10^5 MCS and representative shapes. The final, rounded aggregates remained stable, and the energy was practically constant up to 10^6 MCS (not shown).

Once the structure reaches the metastable state, it can be stabilized by dissolving the supporting gel. In the simulations, this corresponds to increasing the value of γ_{cg}/E_T. Indeed, if in the simulation shown in Fig. 2*A* this quantity is changed to $\gamma_{cg}/E_T = 2$ anywhere in the plateau region, the energy remains constant as long as the simulation is run (results not shown).

Experimental Realization of 3D Structure. To study the feasibility of engineering 3D tissue constructs of prescribed geometry, we have "manually printed" (i.e., embedded) aggregates of living cells into biocompatible gels. As indicated by our model, the ability of aggregates to fuse depends on the mutual properties of the cells and gel. The results of our experiments in Fig. 1 support this prediction. The interfacial tension, γ_{cg} contains three terms, which, in principle, can all be controlled. We performed experiments with fixed cell–cell adhesion and varying gel properties. For the purposes of this study, we used *N*-cadherin transfected CHO cells. Their adhesive properties were quantitatively assessed by measuring aggregate surface tension (for details on the method, see refs. 12, 24, 33, and 34). We used gels with differing chemical composition. The relative importance of cell–cell and cell–matrix interactions has been investigated quantitatively (11).

Results in Fig. 1 *I* and *J* show that collagen at concentration of 1.7 mg/ml is analogous to a permissive scaffold with small γ_{cg}/E_T. Collagen at concentration of 1.0 and 1.2 mg/ml and the RGD containing neurogel match more the definition of the nonpermissive gel with high γ_{cg}/E_T. These gels favor much less (collagen), or not at all (neurogel), the dispersion of the cells into the scaffold, thus facilitating fusion. During our measurements, we did not observe the collapse of the fused rings that, according to the model predictions, should eventually take place (Fig. 2).

The Influence of Scaffold on 3D Structure Formation. The above results demonstrate the well known fact that scaffold properties affect cellular structure (6, 11). The specific mechanism of how the gel influences pattern evolution depends on its detailed chemistry, and in general is not easy to discern.

Cells exert traction forces on their substrates and surrounding 3D matrices (35–38). In the case of collagen, numerous studies of this phenomenon have been performed (39–43). The evolution process in this case has some striking features. As the fusion of aggregates takes place, the pattern noticeably contracts, at

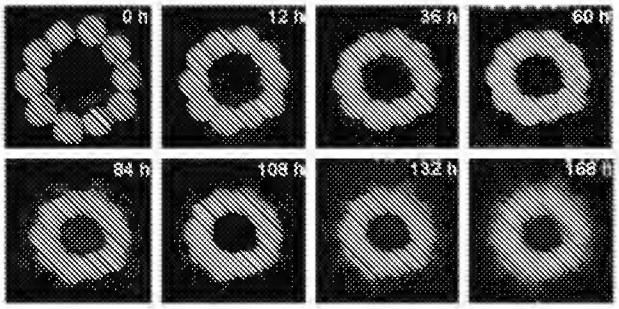

Fig. 3. Time evolution of the cellular pattern in Fig. 1*E*. Note the initial strong contraction (see also Fig. 4). Also note that there are many more cells migrating into the gel than this image might suggest. Because the fluorescent signal of individual cells is much weaker than that of the fused aggregates, they are hard to spot (however, see Fig. 5). The collagen layers above and under the ring are too thin to observe any appreciable cell migration out of the plane of the ring.

least until ≈60 h (Figs. 3 and 4). For higher collagen concentration, contraction is more dramatic, whereas in the case of the neurogel no similar effects were observed (results not shown). Contraction results from the CHO cells pulling on collagen fibers. Furthermore, as aggregates fuse, at some point the pattern assumes a starburst appearance (see spikes at ≈60 h, but not before, in Fig. 5 for the 1.0 mg/ml collagen gel). Cells extend outward from the ring suggesting that by this time a network of radially aligned collagen fibers has developed in the vicinity of the aggregates. (For an explicit visualization of such an array, see ref. 42.) It is remarkable that no similar effect is observed inside the ring even at 144 h (Fig. 5). The probable reason collagen fibers do not align inside the ring is that the vectorial sum of the isotropically acting traction forces is zero. (An analogous cancellation makes the electric field in the interior of a conducting spherical shell to be zero.)

In Fig. 4, we quantified contraction in terms of the total area defined by the outer perimeter of the ring. The curves are exponential fits to the data in the form $A\exp(-t/\tau_{cg}) + B$ (A and B are constants). The quantity τ_{cg} defines a characteristic time scale of contraction. (For the 1.0 mg/ml collagen gel, the one we will use in later analysis, $\tau_{cg} \approx 57$ h.)

Kinetics of Aggregate Fusion. The transparency of collagen allows optically following structure evolution. Fig. 5 shows the time variation of the boundary between two adjacent aggregates in the 1.0 mg/ml collagen gel. A measure of fusion is the instantaneous value of the angle formed by the two aggregates. As aggregates coalesce, the angle between the tangents to their boundaries (drawn from the point where they join) approaches

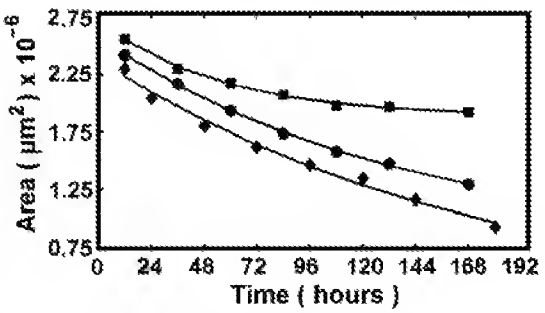

Fig. 4. Cell–matrix interaction induced contraction in collagen gels. The figure shows the change of the entire area inside the outer perimeter of the rings in Fig. 3. Squares, circles, and diamonds stand for collagen concentration 1.0, 1.2, and 1.7 mg/ml, respectively. Curves are exponential fits to the data.

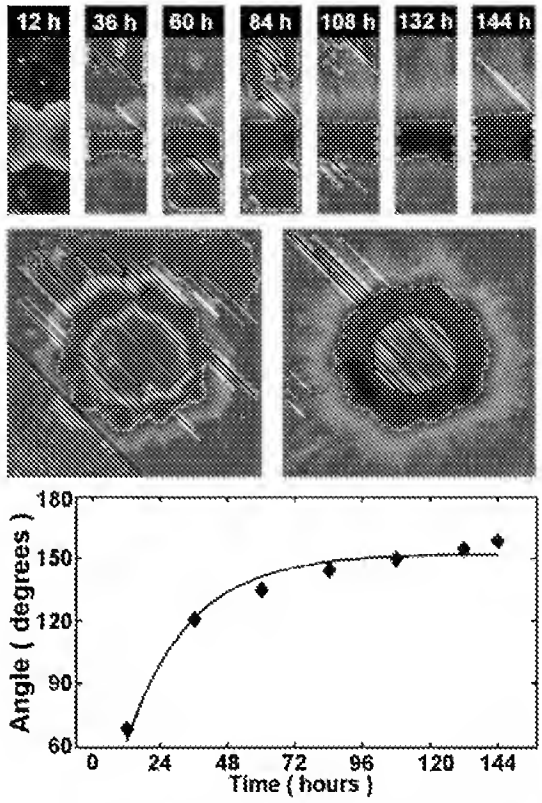

Fig. 5. Time course of aggregate fusion for collagen concentration 1.0 mg/ml. Bright field images of the cellular pattern were acquired with a ×4 objective. (*Top*) Evolution of the cellular boundary between adjacent aggregates. Note the radial, exclusively outward (top) directed migration of cells at around 60 h. (*Middle*) The entire pattern at selected times (*Left*, 36 h; *Right*, 144 h). (*Bottom*) variation of the angle between aggregate boundaries in *Top* as function of time. The curve is an exponential fit to the data (see text for details).

180°. The curve in Fig. 5 is an exponential fit to the data in the form $C[1 - \exp(-t/\tau_{cc})]$ (C is constant), with $\tau_{cc} \approx 23$ h. Here, the quantity τ_{cc} defines a time scale of aggregate fusion.

Discussion

We have manually printed a simple, but nontrivial structure, a ring of spherical aggregates, each containing thousands of cells with specific adhesive properties. We have shown, both experimentally and in computer simulations, that under appropriate conditions the initially contiguous aggregates, positioned along a circle, fuse into a toroidal construct. If aggregates were printed in multiple layers, they would presumably fuse in both the horizontal and vertical directions, thus forming a lumenous organ-like module.

The major outcome of this work is the demonstration that spherical cell aggregates can be used as building blocks in tissue engineering applications. In particular, with the development of automated, computer-aided dispensers or bioprinters (which already exist for the delivery of cells; refs. 13 and 14) they could be used in the capacity of bio-ink.

The biophysical basis for bio-ink is tissue liquidity, a concept proposed by Steinberg (18). The differential adhesion hypothesis (DAH) provides the molecular foundation for tissue liquidity (18, 19). DAH explains the liquid-like behavior of cell populations in terms of tissue surface and interfacial tensions, generated by adhesive and cohesive interactions between the component subunits. *In vitro* experiments have demonstrated that tissue surface tension is a well defined physical parameter, which

characterizes the equilibrium shape of multicellular aggregates. Measured values of the tensions in many cases account for the observed mutual envelopment behavior of tissues (12, 34). *In vivo* experiments give further support to DAH (44, 45).

According to DAH, the lowest energy configuration of any tissue fragment (containing motile cells, uniformly adhesive over their entire surfaces) embedded in a medium to which it adheres weakly, is a sphere. Thus, the final pattern in the 1.0 and 1.2 mg/ml collagen gels and the neurogel should also be a single spherical aggregate. However, as the simulations demonstrate, the system may be trapped in long-lived metastable intermediate states (Fig. 2), which correspond to particular fused conformations. This may provide sufficient time to dissolve the gel, thus freezing the desirable configuration and transferring the resulting tissue construct into a bioreactor for maintenance.

The cell aggregates we used in this work contain cells of only one type. Complex organs contain several cell types. There are indications that using aggregates comprised of heterocellular populations would lead to nontrivial structures. It has been shown, both experimentally (12, 34) and in computer simulations (26, 27), that pattern evolution in sorting is consistent with the predictions of DAH, and is indeed controlled and driven by interfacial tension. Moreover, when the mixture is composed of cells of tissues that are neighbors in normal development, in the course of sorting they recover their physiological configuration (46, 48).

Liquidity has been emphasized for embryonic tissues because it is primarily at this stage of development that tissues and cells must actively move to eventually give rise to organs. Here we used aggregates of *N*-cadherin transfected CHO cells, whose liquidity has been established earlier (49). It is quite likely that when structure formation is induced by the methods described here, aggregates of other cell types (in particular stem cells) will behave similarly to embryonic tissues, as far as their liquidity and ability to fuse is concerned.

Spherical cell aggregates can be made only of adhering cells. Fibroblasts, for example, normally do not adhere to each other directly, only through the extracellular matrix. Such cells can either be temporarily genetically manipulated to express cell adhesion molecules (50, 51) or embedded in a population of adhering cells.

Delivering or printing cell aggregates (instead of individual cells) into 3D scaffolds offers several advantages. Aggregates are prebuilt small tissue blocks, thus their fusion immediately results in 3D structures. Because they contain many thousands of cells, printing time could be dramatically reduced and cell survival greatly improved. Properly designed composite aggregates (with more than one cell type and potentially containing extracellular matrix; i.e., "multicolor bio-ink") can enhance the creation of desired complex tissue constructs. Finally, the inescapable harsh mechanical conditions encountered in presently available printers are more critical for cells than cell aggregates. [Jet-based cell printers (15), due to their small orifice, are presently not appropriate for dispensing aggregates. Devices with the potential to print aggregates of several hundred microns (14) use micropipettes as cartridges with pressure-operated extruders, and thus provide more gentle conditions.]

Our work is based on the analysis of cell–hydrogel interactions in 3D. The computer simulations suggest that for the fusion of the aggregates to take place strict conditions on the embedding gel must be imposed. Our experiments support this prediction. In the case of collagen, because of the tendency of cells to reorganize the matrix, the situation is complex, and the interpretation of the experiments in terms of only gel–aggregate interfacial tension ignores important details. Figs. 4 and 5 imply that pattern evolution involves two distinct time scales, $\tau_{cg} \approx 57$ h and $\tau_{cc} \approx 23$ h for the 1.0 mg/ml collagen matrix, which characterize respectively the dynamical aspects of cell–gel interaction (i.e., how long it takes for the cells to reorganize the matrix) and cell–cell interactions (i.e., how long it takes for the aggregates to fuse). It is the competition between these interactions that determines the final pattern. Because for 1.0 mg/ml collagen $\tau_{cg}/\tau_{cc} \approx 2.5$, contraction is considerably slower than fusion, and the ring has time to stabilize. For 1.7 mg/ml collagen concentration, contraction dominates pattern evolution and the fused ring does not have time to stabilize.

The ideal hydrogel for cell aggregate printing must allow cells to survive and provide favorable conditions for postprinting self-assembly. There already exist several candidates for such gels: thermo-reversible gels (52, 53), photo-sensitive gels (54–56), pH-sensitive gels (57), and gels sensitive to specific molecular entities (58, 59). Detailed studies must be performed to identify the optimal candidate for specific cells or their mixtures.

Our model to describe the observed pattern evolution clearly represents a strong oversimplification of the complex nature of both the cellular and scaffold system. Its major limitation is that it assumes that cells are identical point particles. Thus, in particular, it ignores the change in their shape, a factor known to be important in cell–matrix interactions. Similarly, it treats the embedding gel as a system without internal structure, which is not an adequate characterization of a network of fibers, in particular the one spanning a collagen matrix. Furthermore, cellular rearrangement within the model is exclusively driven by energy minimization (as implemented by the Monte Carlo method), thus, no information can be gained on the true time evolution of the pattern. The entire process is controlled by a single parameter, the aggregate–gel interfacial tension. It is intriguing that, despite these limitations, the similarity between the stimulated and experimentally obtained shapes is so strong. This suggests that our model may incorporate the most salient features of the observed phenomenon. Possible improvement of the model includes the treatment of cells as extended objects, capable of changing their shape. This can be accomplished for example within the large state Potts model (26, 27). Following the true time evolution of the pattern would require the detailed characterization of forces between cells and gel, and necessitate molecular dynamics based simulations instead of the Monte Carlo approach.

In conclusion, we have demonstrated that closely placed cell aggregates in 3D gels can self-organize into metastable tissue constructs of desired shape. It was also shown that adhesive and mechanical properties of the embedding hydrogels are critical for cell aggregate fusion. We have developed a mathematical model that accurately describes our experimental findings. When extended to incorporate more realistic cell and hydrogel properties, it may be used for the design and optimization of scaffold properties. Finally, on the basis of our findings, we have proposed that cell aggregates could be used as self-assembling bio-ink in automated delivery or printing devices.

This work was supported by research grants from the National Science Foundation (to G.F.) and the National Aeronautics and Space Administration (to G.F., V.M., and R.R.M.).

1. Whitesides, G. M. & Grzybowski, B. (2002) *Science* **295**, 2418–2421.
2. Langer, R. & Vacanti, J. P. (1993) *Science* **260**, 920–926.
3. Bonassar, L. J. & Vacanti, C. A. (1998) *J. Cell Biochem. Suppl.* **30–31**, 297–303.
4. Lysaght, M. J., Nguy, N. A. & Sullivan, K. (1998) *Tissue Eng.* **4**, 231–238.
5. Marler, J., Upton, J., Langer, R. & Vacanti, J. (1998) *Adv. Drug Del. Rev.* **33**, 165–182.
6. Griffith, L. G. & Naughton, G. (2002) *Science* **295**, 1009–1014.
7. Wang, Y., Ameer, G. A., Sheppard, B. J. & Langer, R. (2002) *Nat. Biotechnol.* **20**, 602–606.

8. Martin, I., Dozin, B., Quarto, R., Cancedda, R. & Beltrame, F. (1997) *Cytometry* **28,** 2141–2146.
9. Layer, P. G., Robitzki, A., Rothermel, A. & Willbold, E. (2002) *Trends Neurosci.* **3,** 131–134.
10. Steinberg, M. S. (1996) *Dev. Biol.* **187,** 377–388.
11. Ryan, P. L., Foty, R. A., Kohn, J. & Steinberg, M. S. (2001) *Proc. Natl. Acad. Sci. USA* **98,** 4323–4327.
12. Foty, R. A., Pfleger, C. M., Forgacs, G. & Steinberg, M. S. (1996) *Development (Cambridge, U.K.)* **122,** 1611–1620.
13. Liu, V. A. & Bhatia, S. N. (2002) *Biomed. Microdev.* **4,** 257–266.
14. Kachurin, A. M., Stewart, R. L., Church, K. H., Warren, W. L., Fisher, J. P., Mikos, A. G., Kraeft, S. K. & Chen, L. B. (2001) *Proc. Mat. Res. Soc.* **689,** 651–656.
15. Wilson, W. C. & Boland, T. (2003) *Anat Rec.* **272A,** 491–496.
16. Boland, T., Mironov, V., Gutowska, A., Roth, E. A. & Markwald, R. R. (2003) *Anat Rec.* **272A,** 497–502.
17. Mironov, V., Boland, T., Trusk, T., Forgacs, G. & Markwald, R. R. (2003) *Trends Biotechnol.* **21,** 157–161.
18. Steinberg, M. S. (1963) *Science* **137,** 762–763.
19. Steinberg, M. S. and Poole, T. J. (1982) in *Cell Behaviour*, eds. Bellairs, R., Curtis, A. S. G. & Dunn, G. (Cambridge Univ. Press, Cambridge, U.K.), pp. 583–607.
20. Woerly, S., Pinet, E., de Robertis, L., Van Diep, D. & Bousmina, M. (2001) *Biomaterials* **22,** 1095–1111.
21. Woerly, S., Van Diep, D., Sosa, N., de Vellis, J. & Espinosa, A. (2001) *Int. J. Dev. Neurosci.* **19,** 63–83.
22. Israelachvili, J. (1997) *Intermolecular & Surface Forces* (Academic, New York).
23. Benoit, M., Gabriel, D., Gerisch, G. & Gaub, H. E. (2000) *Nat. Cell Biol.* **2,** 313–317.
24. Forgacs, G., Foty, R. A., Shafrir, Y. & Steinberg, M. S. (1998) *Biophys. J.* **74,** 2227–2234.
25. Maheshwari, G., Brown, G., Lauffenburger, D. A., Wells, A. & Griffith, L. G. (2000) *J. Cell Sci.* **113,** 1677–1686.
26. Graner, F. & Glazier, J. A. (1992) *Phys. Rev. Lett.* **69,** 2013–2016.
27. Glazier, J. A. & Graner, F. (1993) *Phys. Rev.* **E47,** 2128–2154.
28. Steinberg, M. S. (1975) *J. Theor. Biol.* **55,** 431–443.
29. Metropolis, N., Rosenbluth, A. W., Rosenbluth, M. N., Teller, A. H. & Teller, E. (1953) *J. Chem. Phys.* **21,** 1087–1092.
30. Press, W. H., Teukolsky, S. A., Vetterling, W. T. & Flannery, B. P. (2002) *Numerical Recipes in C++: The Art of Scientific Computing* (Cambridge Univ. Press, Cambridge, U.K.), 2nd Ed., pp. 275–286.
31. Beysens, D. A., Forgacs, G. & Glazier, J. A. (2000) *Proc. Natl. Acad. Sci. USA* **97,** 9467–9471.
32. Mombach, J. C. M., Glazier, J. A. Raphael, R. C. & Zajac, M. (1995) *Phys. Rev Lett.* **75,** 2244–2247.
33. Foty, R. & Steinberg, M. S. (1997) *Cancer Res.* **57,** 5033–5036.
34. Davis, G. S., Phillips, H. M. & Steinberg, M. S. (1997) *Dev. Biol.* **192,** 630–644.
35. Harris, A. K., Wild, P. & Stopak, D. (1980) *Science* **208,** 177–179.
36. Harris, A. K., Stopak, D. & Wild, P. (1981) *Nature* **290,** 249–251.
37. Vernon, R. B. & Sage, E. H. (1992) *Lab. Invest.* **67,** 807–808.
38. Vernon, R. B. & Sage, E. H. (1996) *J. Cell. Biochem.* **60,** 185–197.
39. Fray, T. R., Molloy, J. E., Armitage, M. P. & Sparrow, J. C. (1998) *Tissue Eng* **4,** 281–291.
40. Vernon, R. B. & Sage, E. H. (1999) *Microvasc. Res.* **57,** 118–133.
41. Korff, T. & Augustin, H. G. (1999) *J. Cell Sci.* **112,** 3249–3258.
42. Sawhney, R. K. & Howard, J. (2002) *J. Cell Biol.* **157,** 1083–1091.
43. Schreiber, D. I., Barocas, V. H. & Tranquillo, R. T. (2003) *Biophys. J.* **84,** 4102–4114.
44. Godt, D. & Tepass, U. (1998) *Nature* **395,** 387–391.
45. González-Reyes, A. & St. Johnston, D. (1998) *Development (Cambridge, U.K.)* **125,** 2837–2846.
46. Townes, P. L. & Holtfreter, J. (1955) *J. Exp Zool.* **128,** 53–120.
47. Techau, U. & Holstein, T. W. (1992) *Dev. Biol.* **151,** 117–127.
48. Ricu, J. P., Kataoka, N. & Sawada, Y. (1998) *Phys. Rev. E* **57,** 924–931.
49. Robinson, E. E., Zazzali, K. M., Corbett, S. A. & Foty, R. A. (2003) *J. Cell Sci.* **116,** 377–386.
50. Steinberg, M. S. & Takeichi, M. (1994) *Proc. Natl. Acad. Sci. USA* **91,** 206–209.
51. Duguay, D., Foty, R. A. & Steinberg, M. S. (2003) *Dev. Biol.* **253,** 309–323.
52. Geong, B., Lee, K. M., Gutowska, A. & An, Y. H. (2002) *Biomacromolecules* **3,** 865–868.
53. Ohya, S., Nakayama, Y. & Matsuda, T. (2001) *Biomacromolecules* **2,** 856–863.
54. Elisseeff, J., Anseth, K., Sims, D., McIntosh, W., Randolph, M., Yaremchuk, M. & Langer, R. (1999) *Plast. Reconstr. Surg.* **104,** 1014–1022.
55. Baier-Leach, J., Bivens, K. A., Patrick, C. W., Jr., & Schmidt, C. E. (2003) *Biotechnol. Bioeng.* **82,** 578–589.
56. Park, Y. D., Tirelli, N. & Hubbell, J. A. (2003) *Biomaterials* **24,** 893–900.
57. Kuiling, D., Woo, S., Demcheva, M. V., Hawes, R. H. & Vournakis, J. N. (1998) *Endoscopy* **30,** S41–S42.
58. Hoffman, A. S. (2002) *Adv. Drug. Deliv. Rev.* **54,** 3–12.
59. Lutolf, M. P., Lauer-Fields, J. L., Schmoekel, H. G., Metters, A. T., Weber, F. E., Fields, G. B. & Hubbell, J. A. (2003) *Proc. Natl. Acad. Sci. USA* **100,** 5413–5418.

major category: Biological Sciences
minor category: Cell Biology and Biophysics

Engineering biological structures of prescribed shape using self-assembling multicellular systems

Karoly Jakab[#], Adrian Neagu[#+], Vladimir Mironov[*], Roger R. Markwald[*] and Gabor Forgacs[#&]

#Department of Physics, University of Missouri, Columbia, MO 65211
+Department of Biophysics and Medical Informatics, Victor Babes University of Medicine and Pharmacy, 1900 Timisoara, Romania
**Department of Cell Biology and Anatomy, Medical University of South Carolina, SC 29425*
&Department of Biology, University of Missouri, Columbia, MO 65211

G. Forgacs
Department of Physics and Biology
University of Missouri
Columbia, MO 65211
Tel: 573 882 3036
Fax: 573 882 4195
e-mail: forgacsg@missouri.edu

# of pages: 22
# of figures: 5

Words in Abstract: 216
Total characters in paper: 46,584

ABSTRACT

Self-assembly is a fundamental process, which drives structural organization in both inanimate and living systems. It is in the course of self-assembly of cells and tissues in early development that the organism and its parts eventually acquire their final shape. Even though developmental patterning through self-assembly is under strict genetic control it is clear that physical mechanisms must underlie the formation of complex structures. Here we show, both experimentally and using computer simulations how tissue liquidity can be employed to build tissue constructs of prescribed geometry in vitro. Spherical aggregates, which consist of many thousand cells and form due to tissue liquidity were implanted contiguously into biocompatible hydrogels in circular geometry. Depending on the properties of the gel, upon incubation the aggregates either fused into toroidal three-dimensional structure or their constituent cells dispersed into the surrounding matrix. The model simulations, which reproduced the experimentally observed shapes indicate that the control parameter of structure evolution is the aggregate-gel interfacial tension. The model-based analysis also revealed that the observed toroidal structure represents a metastable state of the cellular system whose lifetime depends on the magnitude of cell-cell and cell-matrix interactions. Thus these constructs can be made long-lived. We suggest that spherical aggregates composed of organ-specific cells may be used as "bioink" in the evolving technology of organ printing.

Self-assembly is the fundamental process, which generates structural organization across scales (1). Histogenesis and organogenesis are examples of self-assembly processes in which through cell-cell and cell-extra cellular matrix interactions the developing organism and its parts gradually acquire their final shape. In the present work we use both experimental and computational approaches to demonstrate how the self-organizing properties of cells and tissues, the basis for morphogenesis, can be exploited to build three-dimensional (3D) biological structures of prescribed geometry.

Tissue engineering (2-7) offers the opportunity to study self-assembling processes during histo- and organogenesis in vitro under controlled conditions. Tissue engineering aims to not only creating desirable organs, but also to better understand the fundamental mechanisms and principles of biological organization in general and morphogenesis in particular. Classical tissue engineering is based on seeding cells into biodegradable polymer scaffolds or gels, culturing and expanding them in bioreactors for several weeks and finally implanting the resulting tissue into the patient's organism where the maturation of the new organ takes place.

It has recently been suggested to use cell aggregates, instead of individual cells as building blocks in tissue engineering (8,9). Cell aggregates have traditionally been used as a powerful tool to understand the principles of cell-cell (10) and cell-matrix adhesion (11) as well as cell sorting (12). In addition, rapid prototyping technology has successfully been applied for computer-aided deposition of cells in gels in order to create 3D tissue constructs (13,14). We introduce the concept of "bioink", spherical cell aggregates, which upon implantation or "printing" into a scaffold ("biopaper") have the ability to fuse into 3D organ structures (15-17).

The ability of cell aggregates to fuse is based on the notion of tissue fluidity (18,19), according to which embryonic tissues in many respect can be considered as liquids. In particular, in suspension or on non-adhesive surfaces, various multicellular aggregates round up into spherical shape similarly to liquid droplets (12). We hypothesize that closely placed aggregates in appropriately chosen 3D gels can fuse to form tissue constructs of desired geometry.

To demonstrate the feasibility of such a proposition we used aggregates of genetically transformed cells with controlled adhesive properties and arranged them to form a ring in gels of different chemical and mechanical properties. Our results demonstrate that contiguous aggregates under appropriate conditions, defined by the composition of the embedding gel indeed can fuse into structures of specified morphology. We have also constructed and experimentally validated a mathematical model of cell aggregate fusion with strong predictive power.

Taken together these results suggest that cell aggregates can successfully be used as building blocks in tissue engineering technologies. They also provide support for the concept of self-assembling bioink and thus justification for the use of cell aggregates in the evolving organ printing tools.

Materials and Methods

Cell Aggregate Preparation. Chinese Hamster Ovary (CHO) cells transfected with N-cadherin (courtesy of A. Bershadsky, Weizmann Institute, Rehovot, Israel) were infected with histon binding H2B-YFP retrovirus (kindly provided by R.D. Lansford,

Beckman Institute at California Institute of Technology). Confluent cell cultures (3-4x10^6 cells/75 cm^2 TC dish) grown in Dulbecco's Modified Eagle Medium (DMEM, Gibco BRL Grand Island, NY; with 4500 mg/L glucose, L-Glutamine and pyridoxine hydrochloride and supplemented with 10% FBS (US Biotechnologies, Parkerford, PA), 10μg/ml of penicillin, streptomycin, gentamicin, kanamycin, 400μg/ml geneticin and MEM sodium pyruvate) were washed twice with Hanks Balanced Salt Solution (HBSS) containing 2mM $CaCl_2$, then treated for 10 minutes with Trypsin 0.1% (diluted from 2.5% stock, Gibco BRL, Grand Island, NY). Depleted cells were centrifuged at 2500 RPM for 4 minutes. The resulting pellet was transferred into capillary micropipettes of 500 μm diameter, incubated at 37 C^0 with 5% CO_2 for 10 minutes. The firm cylinders of cells removed from the pipettes were cut into fragment (500 μm height), then incubated in 10-ml tissue culture flasks (Bellco Glass, Vineland, NJ) with 3 ml DMEM on a gyratory shaker at 120 RPM with 5% CO_2 at 37°C for 24-36 hours. This procedure reproducibly provides spherical aggregates of similar (~500 μm diameter) size.

Cell Aggregate-Gel Structures. NeuroGel™ (a biocompatible porous poly[N-(hydroxypropil)methacrylamide] hydrogel) disks of 10mm diameter and 2 mm thickness, containing RGD fragments (kindly provided by Stephane Woerly, Organogel Canada, Quebec) were washed three times with DMEM to eliminate the storage medium. This gel has been shown to provide favorable conditions for spinal cord repair (20,21). A 0.5 mm wide, 0.5 mm deep circular groove was cut into a disk, then filled with 10 aggregates, placed contiguously. The groove was refilled with the gel to completely embed the aggregates. This structure was incubated at 37°C, 5% CO_2 for 72 hours in a tissue culture

dish containing 10 ml DMEM, washed with PBS and finally embedded in Tissue-Tek® OCT Compound (Electron Microscopy Sciences, Fort Washington, PA). The structure was slowly cooled (1 C^0/min) to –20 C^0 in a Nalgene freezing container (Nalgene Labware, Rochester, NY). To visualize aggregate fusion, at the end of the experiment cryosectioning was performed with a Reichert 2800N Frigocut cryotome (Reichert Jung, Arnsberg, Germany), yielding 10-16 μm thin slices mounted on microscope slides. Slices were examined on an Olympus IX-70 inverted microscope with fluorescent attachment at 4x magnification.

To tune the strength of cell-gel interaction further fusion experiments were conducted in rat-tail collagen type I (Sigma-Aldrich, St. Louis, MO). Collagen was dissolved in 1N acetic acid then treated with Ham's F12 medium with sodium bicarbonate. Under room temperature this mixture gels in a few minutes depending on concentration. The gel-aggregate structure was achieved by creating a ring of ten aggregates on the top of a previously (almost) solidified collagen layer, then covering with liquid collagen that embeds the aggregates after gelation. These samples were incubated under the same conditions as described above. Working with 1.0 mg/ml and 1.7 mg/ml collagen, the samples were transparent, thus it was possible to follow pattern evolution in time by phase contrast and fluorescent microscopy.

Cell survivability was checked with Trypan Blue (Invitrogen, Carlsbad, CA) at the end of the fusion experiments. A minimal number of uniformly distributed dead cells were found.

Modeling structure formation via cell aggregate fusion. To investigate shape changes of the aggregate structure in gel, we constructed a three-dimensional model, in which the sites of a cubic lattice are considered to be occupied either by cells or by gel volume elements. The total interaction energy or the Hamiltonian of the system is written as

$$H = \sum_{<r,r'>} J(\sigma_r, \sigma_{r'}), \tag{1}$$

where r and r' label lattice sites, and $<r,r'>$ signifies summation over neighboring sites, each pair counted once. First, second and third nearest neighbors are included, and we assume that a cell interacts with the same strength with all the 26 cells it comes into contact with. To specify occupancy, we assign a spin value, σ, to each lattice site with values 0 for a "gel particle" and 1 for a cell. The interaction energy of two neighbors, $J(\sigma_r, \sigma_{r'})$, may take either of the values $J(0,0) = -\varepsilon_{gg}$, $J(1,1) = -\varepsilon_{cc}$ or $J(0,1) = J(1,0) = -\varepsilon_{cg}$. Here the positive parameters ε_{cc}, ε_{gg} and ε_{cg} account for contact interaction strengths for cell-cell, gel-gel and cell-gel pairs, respectively. More specifically, these are mechanical works needed to disrupt the corresponding bonds. (Note that ε_{cc} and ε_{gg} are works of cohesion, whereas ε_{cg} is work of adhesion per bond (22)). The strength of cell-cell interaction may be determined experimentally either directly (23) or by measuring the tissue surface tension (12,24), whereas cell-gel interaction is tunable via the concentration of RGD groups in the gel (6,25) or by the concentration of collagen. The gel-gel "bond energy" is an effective measure of gel

filament density, interaction and stiffness and is determined by the specific chemistry of the gel.

The Hamiltonian in Eq. 1 may be rewritten by separating interfacial and bulk terms in the sum. As a result we obtain

$$H = \gamma_{cg} B_{cg} + \text{const.} \tag{2}$$

Here B_{cg} is the total number of cell-gel bonds, and $\gamma_{cg} = (\varepsilon_{cc} + \varepsilon_{gg})/2 - \varepsilon_{cg}$ is proportional to the cell-gel interfacial tension (22,26,27) or spreading coefficient (28,29). The remaining terms of the Hamiltonian do not change as the cellular pattern evolves.

Our model is inspired by earlier efforts aiming at computer simulations of cell sorting (the morphogenetic phenomenon in which one of two, initially randomly intermixed cell populations sorts out and becomes surrounded by the other). These were mainly concerned with finding the appropriate motility rules (30). Sorting was successfully simulated using the large-Q Potts model (26,27). In our simulations, due to the need to handle large numbers of cells, shape changes of individual cells are presently not accounted for. However, as far as the evolution of the cellular pattern is concerned, we have adopted the same stochastic procedure used in the Potts model-based studies (26,27).

The evolution of the system is followed using Monte Carlo simulations (31), relying on a random number generator of L'Ecuyer with Baym-Durham shuffle (32). The program identifies the cells on the aggregate-gel interface, picks one of them randomly, and exchanges it with an adjacent gel particle chosen by chance. The corresponding

change in adhesive energy, ΔH, is calculated and the new configuration accepted with a probability $P=1$ if $\Delta H \leq 0$ or $P=\exp(-\beta \Delta H)$ if $\Delta H > 0$, where $\beta = 1/E_T$, is the inverse of the average biological fluctuation energy, analogous to the thermal fluctuation energy (33), $k_B T$ (k_B-Boltzmann's constant T- absolute temperature). Whereas in statistical mechanics this energy characterizes thermal agitation in a system of atoms or molecules, in the case of cells it may be thought of as a measure of the spontaneous, cytoskeleton driven motion of cells, able to break adhesive bonds between neighbors via membrane ruffling (34). By definition, a Monte Carlo step (MCS) is completed when each cell in contact with the gel has been given the chance to move once. During each MCS the interfacial sites are selected in random order. The gel boundary is treated as a fixed physical limit of the system and cells are constrained to move within the gel.

Results

Structure formation: simulations. The result stated in Eq. 2 indicates that the evolution of the cellular pattern within the gel is governed by a single parameter, γ_{cg}/E_T, which, for cells with specific adhesive properties, is controlled by the chemistry of the gel. The theoretical analysis shows that once the characteristics of the gel are appropriately tuned, efficient fusion of adjacent aggregates takes place. A gel that promotes effective cell motility lowers the interfacial tension in comparison to the tissue surface tension (i.e. the interfacial tension between an aggregate and surrounding tissue culture medium). This is illustrated in the simulation shown in Fig. 1A-B performed for a low interfacial tension ($\gamma_{cg}/E_T = 0.25$). The cells spread in the bulk of the gel and as a result of their high motility the shape of the cellular pattern evolves towards the lowest

energy state, which corresponds to a uniform distribution of cells within the gel. (The spheroidal structure in Fig. 1B eventually disperses.) Under optimal cell-gel interface properties, expressed in our model by a certain range of the spreading coefficient, fusion occurs resulting in a three-dimensional toroidal structure. An example of this kind is depicted in Fig. 1I-F ($\gamma_{cg}/E_T = 0.9$).

Energetics during structure formation. Some shapes correspond to local minima of the interaction energy: they represent metastable configurations. These are identified from plateaus in the plot of the total interaction energy vs. MCS, and are important for organ engineering, for they can be made long-lived. The initial configuration in Fig. 1I progresses towards such a long-lived metastable state. This is illustrated in more detail in Fig. 2, where the energy of the metastable state is essentially unchanged in the entire interval between 10^4 and 6 x 10^4 MCS. Eventually the fused toroidal state becomes unstable: a particular section of the structure becomes gradually thinner. This corresponds to a slight negative slope of the energy plot, as shown in Fig 2B, and at about 10^5 MCS the torus brakes down. Subsequent massive rearrangements lead to a pronounced energy decrease while the system evolves into three rounded aggregates. These remain stable because large spatial separations hinder their fusion into a single large spheroid. Similar simulations showed that metastability depends both on system size and interaction strengths.

Once the cellular structure reaches the metastable state, it can be stabilized by dissolving the supporting gel. In the simulations this corresponds to increasing the value of the aggregate-gel interfacial tension. Indeed, if in the simulations shown in Fig. 2A,

this quantity is changed to $\gamma_{cg}/E_T = 2$ anywhere in the plateau region, the energy remains constant as long as the simulation is run (results not shown).

Experimental realization of three-dimensional structure. To study the feasibility of engineering three-dimensional tissue constructs of prescribed geometry, we have "manually printed" (i.e. embedded) aggregates of living cells into biocompatible gels following insight form computer simulations. As indicated by our model, the ability of aggregates to fuse depends on the mutual properties of the cells and the gel, as expressed by the parameter γ_{cg}/E_T. The results of our experiments, summarized in Fig. 1 and 3, support this prediction. The spreading coefficient contains three terms, which, in principle, can all be controlled. We performed experiments with fixed cell-cell adhesion and varying gel properties. For the purposes of this study, we used N-cadherin transfected CHO cells. Adhesion between particular cells can quantitatively be assessed, by measuring the surface tension of tissues composed of these cells, as it was done in a number of cases (12, 24, 35). Gel properties were varied by using materials with differing chemical composition. The importance of cell-cell versus cell-matrix interactions has also been investigated quantitatively (11).

Results in Fig. 1C-D show that collagen at concentration of 1.7 mg/ml is analogous to a permissive scaffold with small γ_{cg}/E_T. On the contrary, collagen at concentration of 1.0 mg/ml and the RGD containing neurogel match more the definition of the non-permissive gel with high γ_{cg}/E_T These gels do not favor the dispersion of the cells into the scaffold thus facilitating fusion, as can be seen in Figs. 1E-F, I-J and Fig. 3.

During our measurements we did not observe the collapse of the fused rings that according to the model predictions should eventually happen (see Fig. 2).

Mechanism of 3D structure formation in collagen. It is well known that cells exert traction forces on their surrounding matrices (36-39). This may affect structure evolution, and indeed as Fig. 3 shows the circular configuration markedly contracts at least up to a certain point. The mechanism of structure formation in collagen, as shown in Figs. 1 and 3, can be understood using recent quantitative results on cell-collagen interactions (40-43). In case of a single cell aggregate embedded in collagen cells reorganize the originally homogeneous and isotropic array of collagen fibers. They initially tow the matrix symmetrically from all directions and simultaneously start spreading along them. This results in cell treadmilling with little net cell migration. With time, collagen movement slows down, whereas cell spreading away from the aggregate accelerates. When two aggregates are embedded into collagen, as a consequence of traction collagen fibers align parallel to each other and form a strap between the aggregates with subsequent cell migration along the strap (43).

The structure evolution shown in Fig. 3, although more complicated, is consistent with the earlier findings on cell-matrix interactions. In the configuration of 10 aggregates (Fig. 3), each pair along the diagonal of the ring would give rise to a collagen strap in the absence of the others. Due to symmetry, the cumulative effect of all the aggregates is that no stripes form inside the ring (collagen fibers "do not know" between which aggregates to align). At the same time each aggregate can exert traction on the fibers outside of the ring. As fibers are towed they push on the aggregates. The pattern effectively contracts,

since no counterbalancing structure inside the circle exists. Using the time evolution of the pattern as showed in Fig. 3 (and a similar sequence for the higher collagen concentration, not shown) we measured the area defined by the fluorescent ring as function of time. Results are shown in Fig. 4. As the movement of collagen fibers outside the ring slows down for collagen at concentration of 1.0 mg/ml, the rate of contraction decreases rapidly, but remains almost steady for the higher collagen concentration. The less concentrated collagen preparation represents a thin gel on which the cells' ability to pull and thus migrate is limited (38). If we assume that area contraction is predominantly due to collagen fiber movement, the rate of contraction $\frac{d}{dt}\left[\pi r^2(t)\right] = C(t)$ determined from Fig. 4 allows to obtain a measure for $v(t)$, the instantaneous speed of collagen fiber movement by $v(t) = C(t)/2\pi r(t)$. This speed decreases from its initial value of 0.02 μ/min and 0.04 μ/min to 0.003 μ/min and 0.02 μ/min, respectively for collagen concentrations 1.0 mg/ml and 1.7 mg/ml. These results are consistent with the findings of Sawhney and Howard (43) (these authors used fibroblasts in their studies).

Kinetics of aggregate fusion. Since the transparency of collagen allows to follow structure evolution in time, we were able to quantify the development of the fused ring as shown in Fig. 3. Fig. 5A shows the time evolution of the boundary between two adjacent aggregates in the 1.0 mg/ml collagen gel. Note that up to 60 hours, there is minimal migration of cells into collagen and when migration is pronounced it occurs only outward, but not inward. This may be the indication that no alignment of collagen fibers inside the ring has taken place. A measure of fusion is the angle formed by the two aggregates, whose time dependence is shown in Fig. 5B. As the perimeter of the ring

flattens by the coalescence of aggregates, the angle between their boundaries approaches 180 degrees. The steady increase of this angle shows that cells, at least at the aggregate-gel interface were alive. (Cell viability for the entire construct was checked as explained in the Materials and Methods.)

Discussion

We have manually printed a simple but non-trivial structure, a ring of spherical aggregates, each containing thousands of living cells with specific adhesive properties. We have shown, both in computer simulations and experimentally, that the initially contiguous aggregates positioned along a circle, under appropriate conditions fuse into a toroidal tissue construct. If aggregates were printed in multiple layers (layer-by-layer deposition) they would presumably fuse in both the horizontal and vertical directions, thus forming a vessel-like structure.

The major outcome of this work is the demonstration that spherical cell aggregates can be considered as bioink in the sense that they have the capacity i) to be delivered by computer-aided jet-based or automatic cell dispensor-based "printing" and ii) to consolidate to form "text" or self-assembled histological or tissue constructs.

The biophysical basis for bioink is provided by tissue liquidity. The liquidity of embryonic tissues was proposed by Steinberg (18) as a possible mechanism underlying early developmental patterning. The Differential Adhesion Hypothesis (DAH; 18) provides the molecular foundation for tissue liquidity. DAH explains the liquid-like behavior of cell populations in terms of tissue surface and interfacial tensions, generated by adhesive and cohesive interactions between the component subunits. In vitro

experiments have demonstrated that tissue surface tension is a well-defined intensive physical parameter, which characterizes the equilibrium shape of multicellular aggregates and the measured values of these tensions account for the observed mutual envelopment behavior of the corresponding tissues (12). In vivo experiments give further support to DAH (44-45).

According to DAH the lowest energy configuration of any tissue fragment containing motile cells embedded in a medium to which it adheres weakly, consistent with the notion of tissue liquidity is a sphere. Thus, the final pattern in the 1.0 mg/ml collagen gel and the neurogel should also be a single spherical aggregate. However, as the simulations demonstrate, the system may be trapped in long-lived metastable intermediate states (Fig. 2), which correspond to particular fused conformations. This may provide sufficient time to dissolve the gel thus freezing the desirable metastable configuration and transferring the resulting tissue construct into the bioreactor for maintenance.

Our model and cellular aggregates are clearly oversimplified representations of reality. The model assumes that cells are identical particles, which do not change shape in the course of pattern evolution, which is driven by energy minimization and is controlled by a single parameter, the aggregate-gel interfacial tension. The strong analogy between the stimulated and experimentally obtained shapes nevertheless strongly suggests that our model incorporates the most salient features of the observed structure evolution.

The cell aggregates we used in this work contain cells of only one type; they allow printing only with a single "color". Complex organs contain several cell types. There are many indications that the use of multicolor bioink would lead to highly

nontrivial organ structures. It has been shown by many investigators, both experimentally (12,34,46-48) and using computer simulations (26,27) that sorting follows the behavior of immiscible fluids and is indeed controlled and driven by the interfacial tension. Moreover, when the mixture is composed of cells of tissues that are neighbors in normal development, in the course of sorting they recover their physiological configuration (46,47).

Tissue liquidity has been emphasized for embryonic tissues since it is primarily in this stage of development that tissues and cells must actively move to eventually give rise to organs. Here we used aggregates of N-cadherin trasfected CHO cells, whose liquidity has been established (49). It is quite likely that when structure formation is induced by the methods described here aggregates of other cells types (in particular stem cells) will behave similarly to embryonic tissues, as far as their liquidity and ability to fuse is concerned.

Spherical cell aggregates can be made of only adhering cells. Fibroblasts, for example, normally do not adhere to each other directly only through the ECM. Such cells can either be temporarily genetically manipulated to express cell adhesion molecules (50,51) or embedded in a population of adhering cells.

Printing cell aggregates instead of individual cells offers several advantageous. First, aggregates are pre-built small tissue blocks, thus their fusion immediately results in 3D structures. Second, since they contain many thousands of cells printing time could be dramatically reduced and thus cell survival greatly improved. Third, properly designed composite aggregates (more than one cell type and potentially containing ECM, i.e. multicolor bioink) can enhance the creation of desired complex tissue constructs. Finally,

the inescapable harsh mechanical conditions encountered in the nozzle of the printer are more critical for cells than cell aggregates.

The real challenge for organ printing is not so much placing cells in 3D space, which has already been demonstrated to be technically feasible (13-17), but rather the capacity of these precisely placed cell aggregates to fuse and form histotypic and organotypic structures and then consolidate into mechanically stable and maintainable constructs. The latter is probably not possible without some sort of smart hydrogel. These gels must allow cell aggregates to fuse into the desired geometry. Our data strongly indicate that this can be accomplished only by assuring the right balance between cell-cell and cell-matrix (hydrogel) adhesion, as shown by Ryan et al. (11) for cell aggregate spreading on 2D substrates.

Our work is based on the analysis of cell-hydrogel interactions in 3D. The computer simulations indicate that for the fusion of the aggregates to take place strict conditions on the embedding gel must be imposed. Our experiments show that by tuning the properties of the hydrogel, the fusion of aggregates made of N-cadherin transfected CHO cells could be altered. Collagen type I at concentration of 1.7 mg/ml does not favor aggregate fusion because it is too easy for the cells to migrate into the gel (the interfacial tension, γ_{cg} in the simulations is too small). On the other hand collagen at concentration 1.0 mg/ml or a special neurogel with optimal concentration of RGD fragments (6) allow only restricted motion of cells away from the aggregates and thus promote fusion (γ_{cg} is sufficiently large).

The ideal hydrogel for organ printing must allow cells to survive and must provide favorable conditions for post-printing tissue fusion and self-assembly. There

already exist several candidates for such gels: thermo-reversible gels (52,53), photo-sensitive gels (54-56), pH- sensitive gels (57) and gels sensitive to specific molecular entities (58,59). Detailed studies must be performed to identify the optimal candidate for specific cells or their mixtures. The capacity to predict cell aggregate "fusogenic" behavior and guide the choice of the optimal gel are important attributes of the developed mathematical model.

Several hypotheses have been proposed to explain the locomotive behavior of cells in 3D gels. According to one concept (60) it is the pore size of the gel that determines cell migration. However there is strong evidence that the presence in 3D gels of adhesive sites such as RGD fragments, especially in optimal concentration and arrangement is critical for cell attachment and motion (6, 61-64).

Finally, the mechanical properties of gels are also critical for cell migration (36-43, 65,66). It would be beneficial for tissue engineering applications if the numerous gels now in use could be analyzed in terms of a few relevant physical parameters, as is the case (to an extreme degree) in our simplified model where all matrix properties (both chemical and mechanical) are reduced to a single quantity, the interfacial tension. It is clear, further specially designed experiments are necessary to elucidate this important point.

In conclusion, we have demonstrated that closely placed cell aggregates in 3D gels can self-organize into metastable tissue constructs of desired form. It was also shown that adhesive and mechanical properties of the embedding hydrogels are critical for both cell aggregate fusion and the maintenance of the printed construct. We have developed a mathematical model that can be used for the design and optimization of hydrogel

properties and the prediction of the emerging biological structure. Finally, we have shown both experimentally and theoretically that cell aggregates could be used as self-assembling bioink for evolving organ printing technology.

This work was supported by research grants from NSF (G.F.) and NASA (G.F., V.M., R.M.).

REFERENCES

1. Whitesides, G.M. & Grzyboski, B. (2002) *Science* (2002) **295,** 2418-21.

2. Langer, R., & Vacanti, J. P. (1993) *Science* **260,** 920-926.

3. Bonassar, L. J. & Vacanti, C. A. (1998) *J. Cell Biochem. Suppl.* **30-31**, 297-303.

4. Lysaght, M.J., Nguy, N.A. & Sullivan, K. (1998) *Tissue Eng.* **4**, 231-238.

5. Marler, J., Upton, J., Langer, R. & Vacanti, J. (1998) *Adv. Drug Del. Rev.* **33**, 165-182.

6. Griffith, L. G. & Naughton, G. (2002) *Science* **295,** 1009-1014.

7. Wang, Y., Ameer, G. A., Sheppard, B. J. & Langer, R. (2002) *Nat. Biotechnol.* **20,** 602:606.

8. Martin, I., Dozin, B., Quarto, R., Cancedda, R. & Beltrame, F. (1997) *Cytometry* **28**, 2 141-2146.

9. Layer, P.G., Robitzki, A., Rothermel, A. & Willbold, E. (2002) *Trends Neurosci.* **3**, 131-134.

10. Steinberg, M.S. (1996) *Dev. Biol.* **187,** 377-388.

11. Ryan, P.L., Foty, R.A., Kohn, J. & Steinberg, M.S. (2001) *Proc. Natl. Acad. Sci.* USA **98**, 4323-4327.

12. Foty, R. A., Pfleger, C. M., Forgacs, G. & Steinberg, M. S. (1996) *Development* **122,** 1611-1620.

13. Liu, V.A. & Bhatia, S.N. (2002) *J. Biomed. Microdev.* 4, 257-266.

14. Smith, C.M., Stone, A.L., Parkill, R.L., Steward, R.L., Simplins, M.W., Kachurin, A.M., Warren, W.L. & Williams, S.K. (2003) In: *Society for Biomaterials 29th Annual Meeting Transactions* p.521.

15. Wilson, W.C. & Boland, T. (2003) *Anat Rec.* 272A, 491-496.

16. Boland, T., Mironov, V., Gutowska, A., Roth, E.A. & Markwald, R.R. (2003) *Anat Rec.* **272A**, 497-502.

17. Mironov, V., Boland, T., Trusk, T., Forgacs, G. & Markwald, R.R. (2003) *Trends Biotechnol.* **21**, 157-161.

18. Steinberg, M.S. (1963) *Science* **137**, 762-763.

19. Steinberg, M.S. (1998) *Integrative Biology* **1**, 49-59.

20. Woerly, S., Pinet, E., de Robertis, L., Van Diep, D. & Bousmina, M. (2001) *Biomat.* **22**, 1095-1111.

21. Woerly, S., Van Diep, D., Sosa, N., de Vellis, J. & Espinosa, A. (2001) *Int. J. Devl. Neurosci.* **19**, 63-83.

22. Israelashvili, J. (1997) *Intermolecular & Surface Forces* (Academic Press, New York).

23. Benoit, M., Gabriel, D., Gerisch, G. & Gaub, H. E. (2000) *Nature Cell Biol.* **2,** 313-317.

24. Forgacs, G., Foty, R. A., Shafrir, Y. & Steinberg, M. S. (1998) *Biophys. J.* **74,** 2227-2234.

25. Maheshwari, G., Brown, G., Lauffenburger, D. A., Wells, A. & Griffith, L. G. (2000) *J. Cell Sci.* **113,** 1677-1686.

26. Graner, F. & Glazier, J.A. (1992) *Phys. Rev. Lett* **69**, 2013-2016.

27. Glazier, J.A. & Graner, F. (1993) *Phys. Rev.* **E47**, 2128-2154.

28. Torza, S. and Mason, S.G. (1969). *Science* **163,** 813-814.

29. de Gennes, P.G. (1985) *Rev. Mod. Phys.* **57**, 827-863.

30. Steinberg, M. S. (1975) *J. Theor. Biol.* **55,** 431-443.

31. Metropolis, N., Rosenbluth, A. W., Rosenbluth, M. N., Teller, A. H. & Teller, E. (1953) *J. Chem. Phys.* **21,** 1087-1092.

32. Press, W. H., Teukolsky, S. A., Vetterling, W. T. & Flannery, B. P. (2002) *Numerical Recipes in C++: The Art of Scientific Computing*. 2nd ed., Cambridge Univ. Press, Cambridge. pp. 275-286.

33. Beysens, D. A., Forgacs, G. & Glazier, J. A. (2000) *Proc. Natl. Acad. Sci.* USA **97,** 9467-9471.

34. Mombach, J.C.M., Glazier, J.A. Raphael, R.C. & Zajac, M. (1995) *Phys. Rev. Lett.* **75**, 2244-2247.

35. Foty, R. and Steinberg, M.S. (1997) *Cancer Res.* **57,** 5033-5036.

36. Harris, A.K., Wild, P. & Stopak, D. (1980) *Science* **208**, 177-179.

37. Harris, A.K., Stopak, D. & Wild, P. (1981) *Nature* **290**, 249-251.

38. Vernon, R.B. & Sage, E.H. (1992) *Lab. Invest.* **67**, 807-808.

39. Vernon, R.B. & Sage, E.H. (1996) *J. Cell. Biochem.* **60**, 185-197.

40. Fray, T.R., Molloy, J.E., Armitage, M.P. & Sparrow, J.C. (1998) *Tissue Eng.* **4**, 281-291.

41. Vernon, R.B. & Sage, E.H. (1999) *Microvasc. Res.* **57**, 118-133.

42. Korff, T. & Augustin, H.G. (1999) *J. Cell Sci.* **112**, 3249-3258.

43. Sawhney, R.K. & Howard, J. (2002) *J. Cell Biol.* **157**, 1083-1091.

44. Godt, D. & Tepass, U. (1998) *Nature* **395**, 387-391.

45. González-Reyes, A. & St. Johnston, D. (1998) *Development* **125**, 2837-2846.

46. Townes, P.L. and Holtfreter, J. (1955) *J. Exp Zool.* **128**, 53-120.

47. Techau, U. & Holstein, T.W. (1992) *Dev. Biol.* **151**. 117-127.

48. Rieu, J.P., Kataoka, N. & Sawada, Y. (1998) *Phys. Rev.* E **57**, 924-931.

49. Robinson, E. E., Zazzali, K. M., Corbett, S. A. & Foty, R. A. (2003) *J. Cell Sci.* **116,** 377-386.

50. Steinberg, M.S. and Takeichi, M. (1994). *Proc. Natl. Acad. Sci.* USA **91**, 206-209.

51. Duguay, D., Foty, R. A. & Steinberg, M. S. (2003) Dev. Biol. 253, 309-323.

52. Leong, B., Lee, K.M., Gutowska, A. & An, Y.H. 2002 *Biomacromolecules* **3**, 865-865.

53. Ohya, S., Nakayama, Y. & Matsuda T. (2001) *Biomacromolecules* **2**, 856-863.

54. Elisseeff, J., Anseth, K., Sims, D., McIntosh, W., Randolph, M., Yaremchuk, M. & Langer, R. (1999) *Plast Reconstr Surg.* **104**, 1014-22.

55. Baier-Leach, J., Bivens, K.A., Patrick, Jr. C.W. & Schmidt, C.E. (2003) *Biotechnol. Bioeng.* **82**, 578-89.

56. Park, Y.D., Tirelli, N. & Hubbell, J.A. (2003) *Biomaterials* **24**, 893-900.

57. Kulling, D., Woo, S., Demcheva, M.V., Hawes, R.H. & Vournakis, J.N.(1998) *Endoscopy* **30**, S41-2.

58. Hoffman, A.S. (2002) *Adv. Drug. Deliv. Rev.* **54**, 3-12.

59. Lutolf, M.P., Lauer-Fields, J.L., Schmoekel, H.G., Metters, A.T., Weber, F.E., Fields, G.B. & Hubbell, J.A. (2003) *Proc. Natl. Acad. Sci.* USA **100**, 5413-5418.

60. Nehls, V. & Herrmann, R. (1996) *Microvasc. Res.* **51**, 347-64.

61. Stile, R.A. & Healy, K.E. (2001) *Biomacromolecules* **2**, 185-94.

62. Rowley, J.A. & Mooney D,J. (2002) *J. Biomed. Mater. Res. 60*, 217-23.

63. VandeVondele, S., Voros, J. & Hubbell J.A. (2003) *Biotechnol. Bioeng.* **82**, 784-90.

64. Lutolf, M.P., Weber, F.E., Schmoekel, H.G., Schense, J.C., Kohler, T., Muller, R. & Hubbell,J.A. (2003) *Nat. Biotechnol.* **21**, 513-518.

65. Manoussaki, D., Lubkin, S.R., Vernon, R.B. & Murray, J.D. (1996) *Acta Biotheor*. **44**, 271-82.

66. Lubkin, S.R. & Li, Z. (2002) *Biomechan. Model. Mechanobiol*. (2002) **1**, 5-16.

Figure Captions

Fig. 1. Initial (upper row) and final (lower row) cell aggregate configurations in the simulations and in the various biocompatible gels. Panels A-B and E-F correspond to simulations with $\gamma_{cg}/E_T = 0.25$ and $\gamma_{cg}/E_T = 0.9$, respectively. The ten aggregates, each containing 925 cells are one cell diameter from each other in the starting configurations. The final configurations shown in B and F are reached after 25,000 and 50,000 MCS, respectively. Panels C-D, G-H and I-J correspond to CHO cell aggregates embedded in collagen gel of concentration 1.7 mg/ml and 1.0 mg/ml and a neurogel with RGD fragments, respectively. The nuclei of the cells are fluorescently labeled (see Materials and Mehtods) and the images of the cellular patterns were acquired with a 4x objective. The average diameter of the aggregates is 500 μ.

Fig. 2. Metastable configuration at $\gamma_{cg}/E_T = 1.1$; **(A)** Fusion of 16 contiguous aggregates (123 cells each) takes place within the first 5000 MCS. The plateau of the energy vs. MCS corresponds to the thin ring conformation with an average height of 5 cell diameters. **(B)** The evolution of the energy during 5×10^5 MCS and representative shapes. The final, rounded aggregates remained stable, and the energy practically constant up to 10^6 MCS (not shown).

Fig. 3. Time evolution of the cellular pattern in Fig. 1C. Note the initial strong contraction (see Fig. 4). Also note there are many more cells migrating into the gel than this image might suggest. Since the fluorescent signal of individual cells is much weaker than that of the fused aggregates they are hard to spot (see however Fig. 5).

Fig. 4. Cell-matrix interaction induced contraction in collagen gels. The figure shows the change of the entire area inside the outer perimeter of the rings in Fig. 3. Since few cells migrate into the gel, their effect on the area has been ignored. Squares and diamonds stand for collagen concentration 1.0 mg/ml and 1.7 mg/ml, respectively.

Fig. 5. Time course of aggregate fusion for collagen concentration 1.0 mg/ml. Upper panel. The evolution of the cellular boundary between adjacent aggregates. Bright field images were acquired with a 4x objective. Lower panel. Variation of the angle between aggregate boundaries as function of time.

Fig. 2

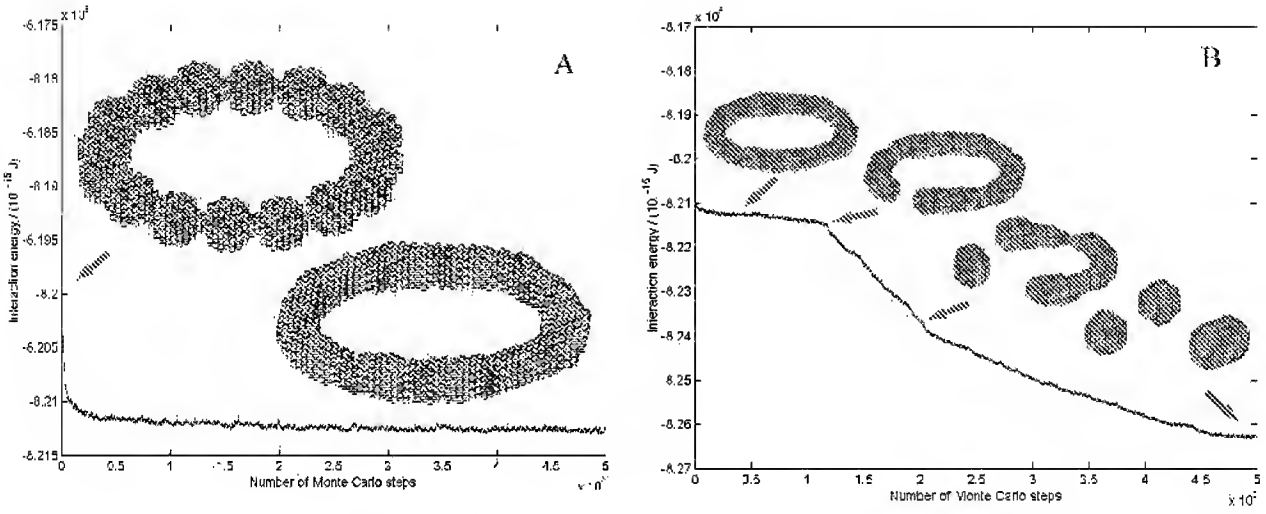

Fig. 3.

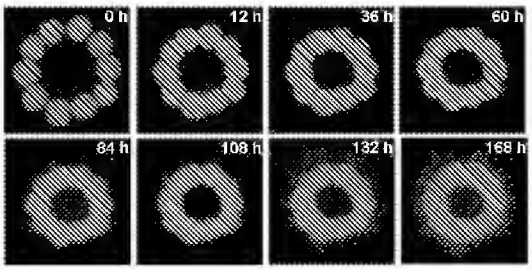

Fig. 4

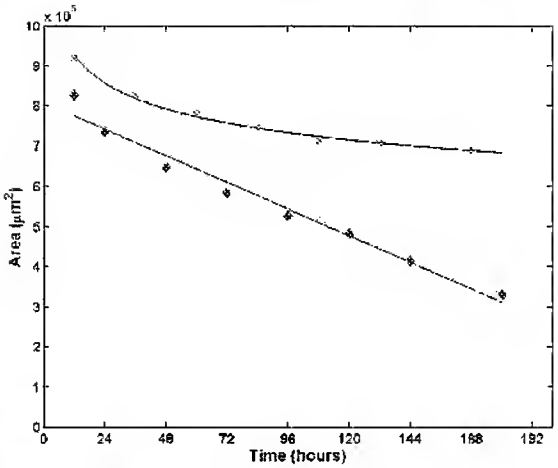

Fig. 5.